Lawrence Livermore Laboratory

$Conf - 75 1130 - 6$

MASTER

STABILITY AND SYMMETRY REQUIREMENTS
OF ELECTRON AND ION BEAM FUSION TARGETS

R. O. Bangerter, J. D. Lindl,

C. E. Max, and W. C. Mead

October 14, 1975

STABILITY AND SYMMETRY REQUIREMENTS

OF ELECTRON AND ION BEAM FUSION TARGETS*

R. O. Bangerter, J. D. Lindl, C. E. Max, and W. C. Mead

Lawrence Livermore Laboratory, Livermore, California 94550

Abstract

Considerations of hydrodynamic stability impose severe restrictions on the design of electron and ion beam imploded fusion targets. Furthermore, in order to obtain a sufficiently spherical implosion, many target designs require electron or ion beams having a high degree of spherical symmetry.

We have studied the stability and symmetry requirements of several recently proposed target designs by numerical simulation using the computer program LASNEX.

The ion beam targets we have studied are more vulnerable to instability than the electron beam targets.

I. Stability

The familiar phenomenon of Rayleigh-Taylor instability occurs when two fluids of density ρ_1 and ρ_2 ($\rho_1 \neq \rho_2$) are placed in contact and accelerated in a direction normal to the interface and directed toward the denser fluid. Specifically, let us assume an acceleration a along the z-axis. If a perturbation of the form $\eta_0 \sin kx$ is applied to an interface at $z = z_0$ the amplitude η at time t is given by

$$\eta = \eta_0 e^{\gamma t} \quad , \qquad \qquad \qquad (1)$$

where $\qquad \gamma = \sqrt{\alpha k a} \qquad \qquad \qquad (2)$

and $\qquad \alpha = \dfrac{\rho_2 - \rho_1}{\rho_2 + \rho_1}$

is the Atwood number. In this case we assume that the fluid of density ρ_2 occupies the region $z > z_0$ so that exponential growth occurs when $\rho_2 > \rho_1$ and $a > 0$.

Equation (1) is valid for $\eta \lesssim \lambda = 2\pi/k$. For $\eta \gtrsim \lambda$ the growth rate becomes more nearly linear in time.[1]

In this paper we consider only spherical fusion targets. In this case we expand the perturbation in spherical harmonics[2] of order ℓ and replace k in Equation (2) by $k \cong \ell/r$ where r is the radius of the interface.

There are at least three cases in typical electron and ion beam fusion targets where Rayleigh-Taylor instability is likely to play an important role. These are shown in Fig. 1.

Case I occurs when an initially uniform spherical shell is heated on the outside by an electron or ion beam. The region in which the beam is deposited expands, producing a low density medium which accelerates the denser material lying inside of the beam deposition region. It might be expected that Equation (2) would not be valid in this case, since one does not expect a density discontinuity but a more gradual density transition. If the density transition between ρ_1 and ρ_2 is exponential, such that

$$\rho = \begin{cases} \rho_1 & z \leq z_0 \\ \rho_1 e^{\beta(z-z_0)} & z_0 < z < z_1 \\ \rho_2 & z_1 \leq z \end{cases}$$

where z_1 is chosen to insure the continuity of ρ, it can be shown[3] that one must make the replacement

$$k \rightarrow \frac{k\beta}{k+\beta} \tag{3}$$

in equation (2).

Case II can occur in target designs having an initial density discontinuity.

Case III occurs near the end of an implosion when the pressure in a relatively light fuel region becomes sufficiently great to decelerate the dense pusher surrounding the fuel.

In Cases I and II the effect of the instability depends on the wavelength. If the wavelength is sufficiently large the growth rate

will be too small to be of any consequence. If the wavelength is comparable to the shell diameter the results will be gross shell distortion, and are coupled to the symmetry requirements of the incoming beam. If the wavelength is much shorter than the shell thickness,[4] saturation of exponential growth will occur before the amplitude becomes of sufficient size to destroy the shell. The effects of turbulent transport and mixing could alter the implosion behavior, but these effects are not included in our treatment.

Perturbations having wavelengths comparable to the shell thickness are expected to be most destructive, since they can grow exponentially to amplitudes of the order of the shell thickness and cause shell break-up. Figure 2 illustrates these wavelength domains for a typical shell.

Similar comments apply to Case III instability if we replace shell thickness by fuel radius.

In fusion targets one might expect Equation (2) to be substantially modified by such things as thermal transport and ablation. We have, therefore, studied the behavior of a number of suggested target designs using the 2-dimensional Lagrangian computer code LASNEX,[5] written by George Zimmerman. This code includes electron and ion deposition, energy transport, and separate electron, ion, and radiation temperatures. As options one may also include multigroup photon and particle transport and magnetic field physics, although we have not done this in our simulations.

We believe the most serious defficiencies of our calculations involve the particle deposition. We have assumed classical energy loss

neglecting self-generated fields, plasma effects, and temperature depen-
dence. Also in the current version of LASNEX, the deposition is calcu-
lated along the radial Lagrangian grid lines. This is incorrect when
the mesh becomes distorted. These defects are currently being eliminated.

The five target designs[6] described in Figures 3a-e and Table I
have been chosen as case studies. Using LASNEX we have been able to
study instability Case I for all designs and Case II for design E. In
most cases we impose a shell thickness perturbation equal to about 1
part in 10^6 of the initial shell radius using zoning similar to that
shown in Fig. 4. This initial amplitude is sufficiently large to dominate
over numerical noise and sufficiently small to allow large growth factors
satisfying the conditions $\eta \ll \lambda$.

Test cases indicate that using only 4 angular zones per wavelength
reduces the growth rate to about 0.8 times its analytic value.[7] Most of
our conclusions are insensitive to this size of variation in growth
rate. Also, using only 4 zones per wavelength effectively suppresses
the growth of modes of higher order than the one under study. For these
reasons, and for computer economy, most problems have been run with 4
zones per wavelength. The thickness δr of the radial zones must be chosen
to satisfy the condition $k\delta r < 1$. This results from the fact that the
perturbation extends a distance $\sim 1/k$ beyond the unstable interface.

Figures 5 to 8 are frames from a movie showing the unsuccessful
implosion of the low power target design A. In this case $\ell = 200$ and
only the outside shell is shown.

Figure 9 shows the shell thickness as a function of time together

with the r.m.s. amplitude[8] of the instability. The dashed curve is a
simple calculation using equation (1) scaled by the ratio of the instan-
taneous density to the initial density in order to account for compres-
sional effects. The growth is evidently catastrophic. Furthermore, we
assumed an initial r.m.s. perturbation of only 7Å. This is rather small.
In practice, it seems feasible to manufacture targets with surface pertur-
bations between 50 and 100 Å, although ∿ 10 Å may be possible.[9]

Figure 10 refers to target design B. Because of its small radius
and large shell thickness, it is probably the most stable design of its
type to appear in the literature. Our calculations indicate that this
target survives Case I instability for $\ell = 100$. We have also simulated
$\ell = 200$ with the same conclusion. In these calculations we had diffi-
culty in satisfying the $k\delta r < 1$ criterion with a reasonable number of
zones. Since the temperature effect on ion stopping power has not been
taken into account, and since we may well start from a 100 Å pertur-
bation, the survival of this target should be considered tentative.

Figures 11 and 12 illustrate the behavior of designs C and D.
The behavior of these targets imploded by 1 MeV electrons is dramat-
ically different than the ion imploded designs A and B. Figure 13 repre-
sents the deposition profiles for 10 MeV protons and 1 MeV electrons in
gold. This difference in deposition profile results in rather different
density profiles as shown in Fig. 14. Fig. 14 corresponds to a time
about midway through the implosion. In the electron case $k \gg \beta$ so that
relation (3) gives $k \rightarrow \beta$ and the growth rate becomes independent of ℓ, as
seen in Figs. 11 and 12. In fact, the lower order perturbations are
shown growing slightly more rapidly than the higher order. We believe

this to be due to zoning difficulties associated with the $k\delta r < 1$ criterion
at late times. There is thus some point in time at which the validity
of the calculation breaks down. Before this time the growth rates are
in reasonable agreement with that predicted by Relation (3). Case I
instability thus seems to be unimportant for 1 MeV electron beam implo-
sions. Unfortunately the electron deposition profile that results in
such benign instability is inefficient in terms of energy requirements.

Target design E survives both Case I and Case II instability.
The Atwood number at the Fe-Au interface is 0.25 to 0.4 during most of
the implosion, and furthermore, the acceleration is relatively low since
the unstable interface is located relatively far out in the ablation
region.

We now turn briefly to the question of Case III instability.
This has been analyzed for electron and ion beam targets using the concept
of the free-fall line. This model in its simplest form rests on the
assumption that no material from a high Z pusher can achieve a velocity
greater than the maximum velocity of the pusher, and thus can arrive at
the center of the target no earlier than time t_o defined in Fig. 15.
If ignition occurs before $t = t_o$ it is assumed that the implosion will
survive the instability. Fig. 15 corresponds to target C.

Roughly 2% of the yield of target C has occured by $t = t_o$, at
which time the temperature of the fuel was about 5 keV. Comparison
with other targets is shown in Table II. We have been unable to quantify
the degradation of burn caused by Case III instability, but the above
analysis provides a rough comparison of the various targets.

II. Symmetry

As mentioned above, the concepts of stability and symmetry are closely related. Shell thickness perturbations of $\ell \sim 100$ quite clearly belong in the realm of stability problems, while shell thickness perturbations having $\ell \sim 2$ are normally considered to be symmetry problems.

Low order symmetry perturbations can be produced by variations in radius, thickness, density, beam power, or time jitter in multiple beams. For example, one expects a two beam target irradiation scheme to have $\ell = 1$ jitter asymmetry, as well as $\ell = 1$ and $\ell = 2$ beam power asymmetry.

Because of fuel turbulence induced by asymmetries, we have had some difficulty in studying this problem with our Lagrangian code LASNEX. However, our 2-D LASNEX calculations indicate that smoothing effects such as thermal conduction have little effect on an $\ell = 2$ perturbation. Because of this fact it is possible to make some rather general statements.

We define convergence ratio as r_i/r_f, where r_i is the initial radius of the outermost pusher, and r_f is the final compressed radius of the fuel. Assume a small angle dependent variation δE in the energy E deposited in some region of target. From a variety of simple models one expects that the variation δV in pusher velocity V to be given by $\delta V/V = c \, \delta E/E$ where c is of order unity.

In order to achieve a large convergence ratio the pusher must move a distance $\sim r_i$. Thus, a perturbation in velocity will result in a radial perturbation $\delta r = r_i \, \delta V/V = cr_i \, \delta E/E$. We expect degradation of the implosion when $\delta r \sim r_f$ or $r_f/r_i \sim c \, \delta E/E$. We thus obtain the rule that the required energy symmetry is proportional to, and roughly equals the

reciprocal of the convergence ratio. Similar arguments can be made
for other types of asymmetries. An $\ell = 2$ perturbation can be crudely
simulated by running two 1-D LASNEX calculations representing slightly
different input powers at the pole and equator of the target. By this
method we obtain $\delta r/r_f \sim 0.5$ for a 5% power difference on target B. This
is shown in Fig. 16. The convergence ratio of target B is about 20, so
that the LASNEX results are in agreement with our simple calculations
for $c \sim 1/2$. The results for other targets are given in Table III.

In these examples it seems likely that an $\ell = 2$ fractional energy
perturbation of r_f/r_i would degrade but not destroy thermonuclear burn,
however, considerably more work is needed in this area.

Conclusions

We find that 1 MeV electron beam targets are rather invulnerable to stability problems. This is a result of the broad deposition profile which produces small density gradients and large shell thickness. By contrast, ion beams produce larger density gradients and thinner shells, and consequently suffer more severe instability damage.

Our preliminary symmetry results confirm the simple rule that the required energy symmetry is roughly equal to the reciprocal of the convergence ratio of the target. Thus symmetry requirements are more stringent for the large, low-power targets having high convergence ratios.

REFERENCES

1. An exact description of large amplitude Rayleigh-Taylor instability is extremely complex. See W. P. Crowley, University of California Report UCRL-72650 (1970).

2. M. S. Plesset, J. of Appl. Phys. 25, 96 (1954).

3. R. LeLevier, G. Lasher, and F. Bjorklund, University of California Report UCRL-4459 (1955).

4. In this paper we have arbitrarily defined shell thickness to be measured between the points where the density of the shell drops to 0.2 times its maximum value.

5. G. B. Zimmerman, University of California Report UCRL-74811 (1973).

6. Targets B, D, and E are described in the following references: M. J. Clauser, PRL 34, 570 (1975); M. J. Clauser, PRL 35, 848 (1975); M. A. Sweeney and M. J. Clauser, Applied Phys. Lett. 27, 483 (1975). Targets A and C were designed by our group at Lawrence Livermore Laboratory.

7. J. D. Lindl and W. C. Mead, PRL 34, 1273 (1975); W. C. Mead and J. D. Lindl, University of California Report UCRL-77057 (1975).

8. The amplitude is measured by calculating r.m.s. deviation of Lagrangian grid line from its mean radius along a symmetry direction.

9. Charles D. Hendricks, Lawrence Livermore Laboratory, private communication.

FIGURE CAPTIONS

Figure 1.   Three cases in which Rayleigh-Taylor instability can occur
in electrons or ion beam fusion targets.

Figure 2.   Behavior of low intermediate, and large ℓ perturbations,
showing some intermediate ℓ value to be the most destructive.

Figure 3.   Five target designs studied.

Figure 4.   Lagrangian mesh for a typical problem. The perturbation is
greatly magnified and only a few radial zones are shown.

Figures 5-8.   Frames from a movie to be presented with talk. The movie
shows the unsuccessful implosion of target A.

Figure 9.   Perturbation amplitude (r.m.s.) and shell thickness as a
function of time for target A.

Figure 10.   Perturbation amplitude (r.m.s.) and shell thickness as a
function of time for target B. The amplitude is measured at
a given mesh line. This results in a small amplitude at early
times. The initial shell thickness perturbation is indicated
by an arrow.

Figure 11.   Perturbation amplitude (r.m.s.) and shell thickness as a
function of time for target design C. The amplitude is the
amplitude of the unstable interface and does not represent a
fixed mesh line since the beam voltage varies as a function
of time for this target design.

Figure 12.   Amplitude (r.m.s.) of unstable interface for target design D.
The wavy line represents the point at which the $k \, \delta r < 1$
criterion is no longer satisfied.

Figure 13.　Deposition profiles for 1 MeV electrons and 10 MeV protons on gold. The incoming electrons were distributed as $\cos\theta$ where θ is the angle with respect to the radial direction. The angular distribution of protons corresponds to a proton beam temperature of 10 eV focused from a sphere 50 cm from the target.

Figure 14.　Density as a function of radius for targets B and D imploded with 10 MeV protons and 1 MeV electrons respectively. These curves are taken at a time of 3.7 ns. This is roughly half way through the implosion.

Figure 15.　Outer radius of fuel as a function of time for target C. The slope of the free-fall line represents the maximum velocity of the pusher-fuel interface.

Figure 16.　Outer radius of fuel as a function of time for power inputs P and P + δP differing by 5% on target B.

TARGET DESIGNS

Target	Beam	Voltage (MeV)	Outside radius (mm)	Peak power (TW)	Input energy (kJ)	Output energy (kJ)
A	Alpha	5	1.07	8	35	30
B	Proton	10	0.72	110	1070	1100
C	Electron	1	2.68	250	4400	5400
D	Electron	1	1.20	1200	6280	7700
E	Electron	1	1.44	400	3200	7860

TABLE I

FREE FALL ANALYSIS SHOWS ION BEAM TARGET AND MULTIPLE
SHELL ELECTRON BEAM TARGET HAVE SUPERIOR IGNITION
CHARACTERISTICS.

	Target	Beam	Percent yield at $t = t_0$	Fuel temperature at $t = t_0$
B	Single shell	10 MeV protons	2.6	4.4
C	Multiple shell	1 MeV electrons	2.1	5.4
D	Single shell	1 MeV electrons	0.55	3.1
E	Fe on Au shell	1 MeV electrons	0.48	3.0

TABLE II

RESULTS OF SYMMETRY CALCULATIONS

Target	$\delta P/P$	r_i/r_f	$\delta r/r_f$	C
B	0.05	23	0.50	0.44
C	0.01	75	0.36	0.48
D	0.05	13	0.24	0.36
E	0.05	22	0.45	0.42

TABLE III

THREE POSSIBLE CASES OF RAYLEIGH-TAYLOR INSTABILITY

Case I   Case II   Case III

Beam deposition region

Low density

High density

Material A

Material A

Material B

Material A

$\downarrow \vec{a}$

$\downarrow \vec{a}$

$\uparrow \vec{a}$

High density pusher

Low density fuel
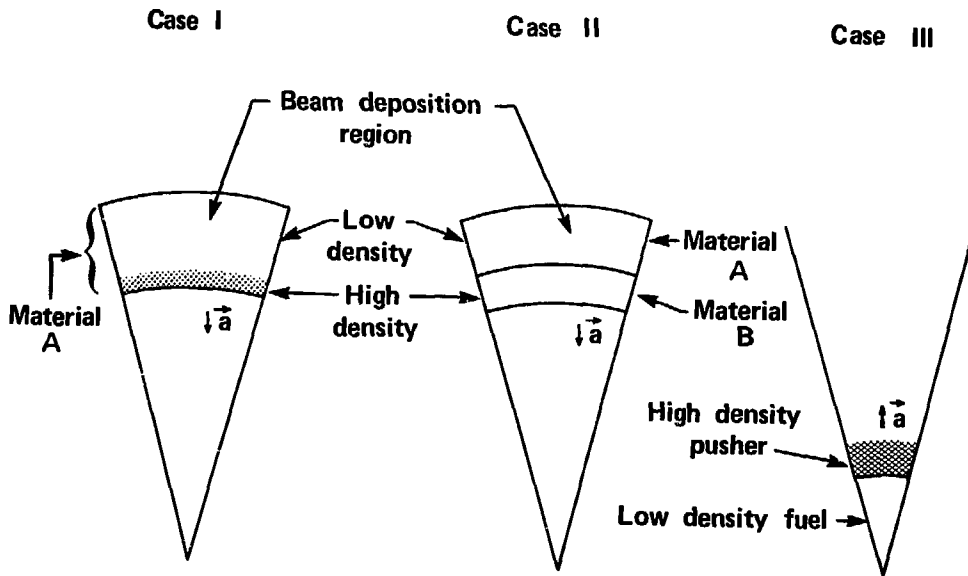
FIGURE 1

DIAGRAM SHOWING INTERMEDIATE ℓ VALUE TO BE MOST DESTRUCTIVE.
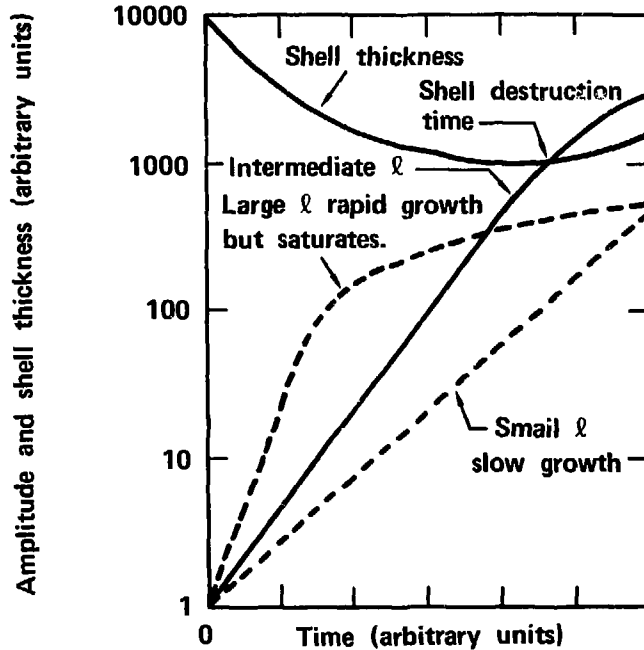
FIGURE 2
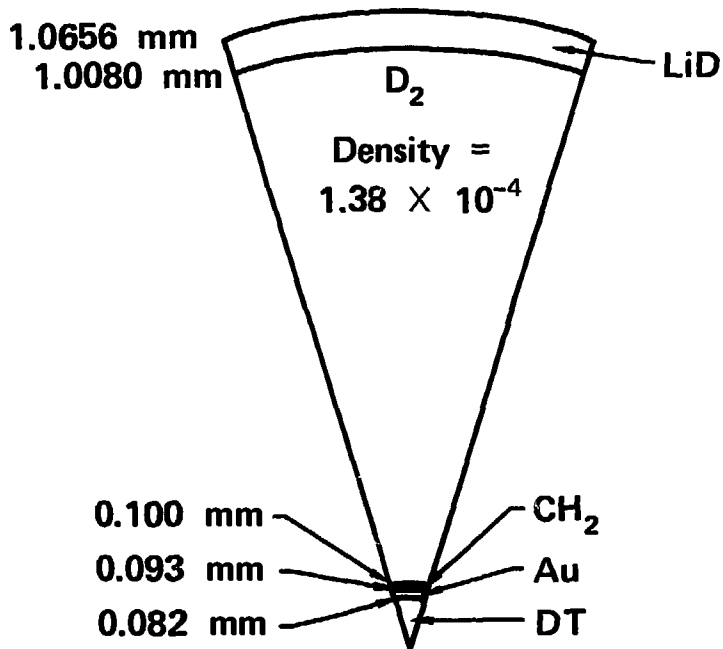
FIGURE 3a

TARGET DESIGN B   10 MeV PROTON BEAM

0.72 mm

Au

0.50 mm

10 μg

DT
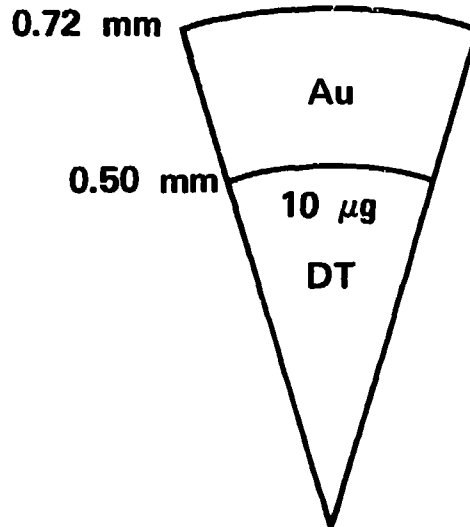
FIGURE 3b

TARGET DESIGN C   1 MeV ELECTRON BEAM

2.6784 mm — Fe

2.3040 mm — D_2 Density = 10^{-3}
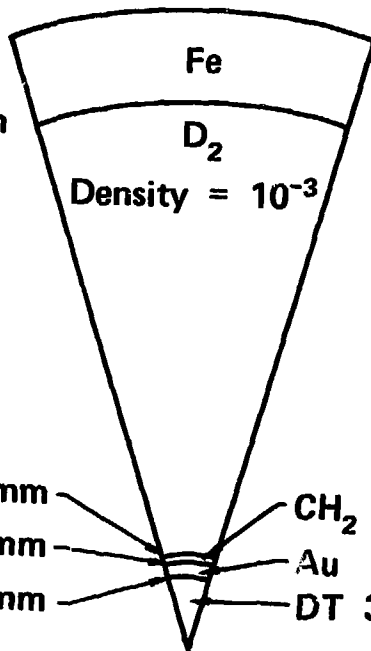
0.3997 mm — CH_2
0.3720 mm — Au
0.3283 mm — DT 31.1 μg

FIGURE 3c

TARGET DESIGN D   1 MeV ELECTRON BEAM

1.2 mm — Au

1.0 mm — 100 μg DT
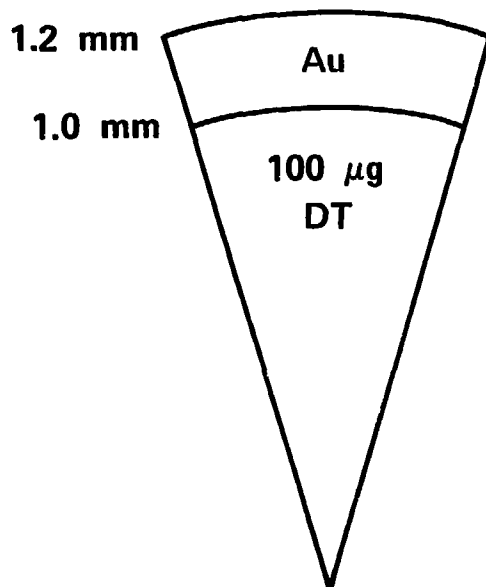
FIGURE 3d

TARGET DESIGN E   1 MeV ELECTRON BEAM

1.44 mm

Fe

1.10 mm

Au

1.00 mm

50 μg

DT
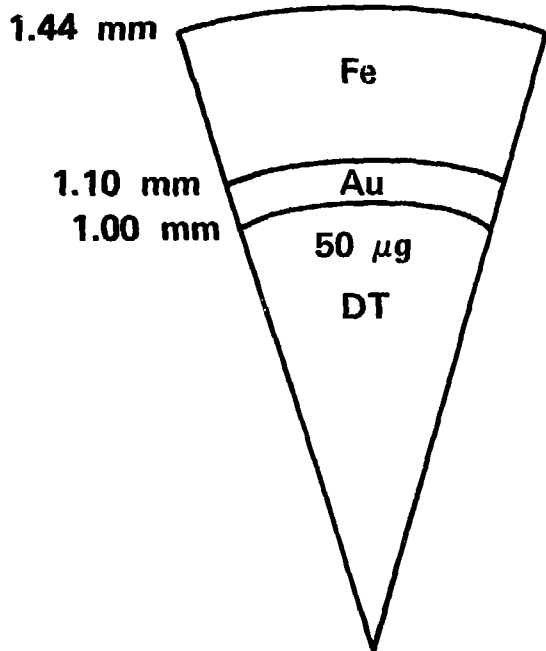
FIGURE 3e

LAGRANGIAN MESH FOR A TYPICAL PROBLEM

Typically ~100 radial zones. The radial zone thickness must satisfy $k\delta r < 1$ at the unstable interface.
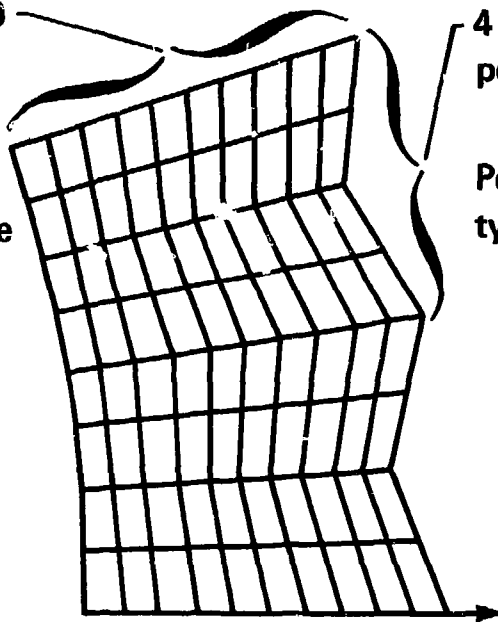
4 angular zones per wavelength

Perturbation is typically ~10 Å

Axis of rotation

FIGURE 4

TIME =   2.045   ALPHA-5MEV   CYCLE=   300.0
ZO=   .050   ZMX=   .110   DR/DZ=   .20
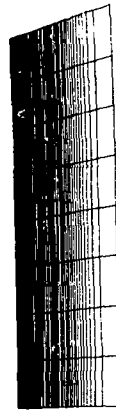
FIGURE 5

TIME = 5.413   ALPHA-5MEV   CYCLE =   1300.0
ZC =   .050   ZMX =   .110   DR/DZ =   .20
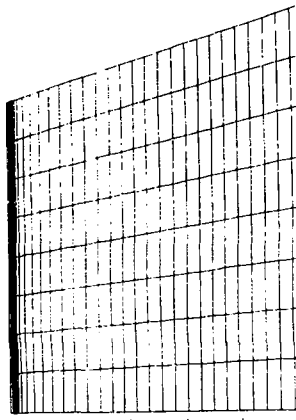
FIGURE 6
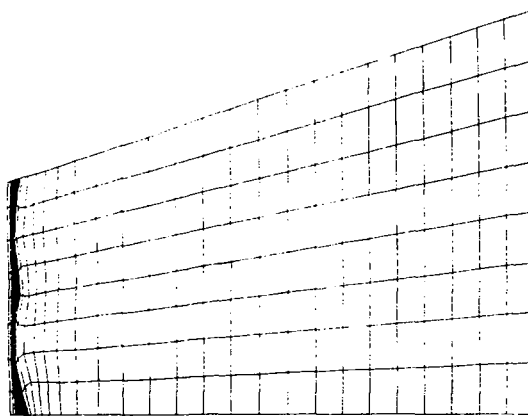
TIME =   6.861   ALPHA-5MEv   CYCLE =   1550.0
ZO=   .050   ZMX=   .110   DR/DZ=   .20
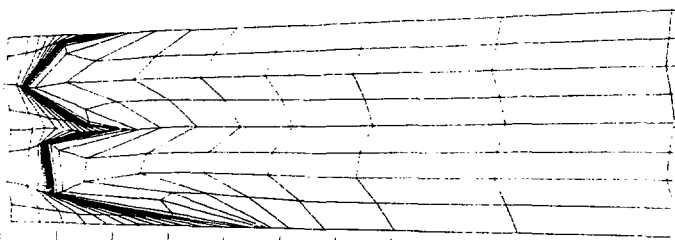
FIGURE

TIME =   7.591   ALPHA-5MEV   CYCLE =   1725.0
ZO =   .050   ZMX =   .062   DR/DZ =   1.00

FIGURE 8

TARGET DESIGN A – TARGET FAILS
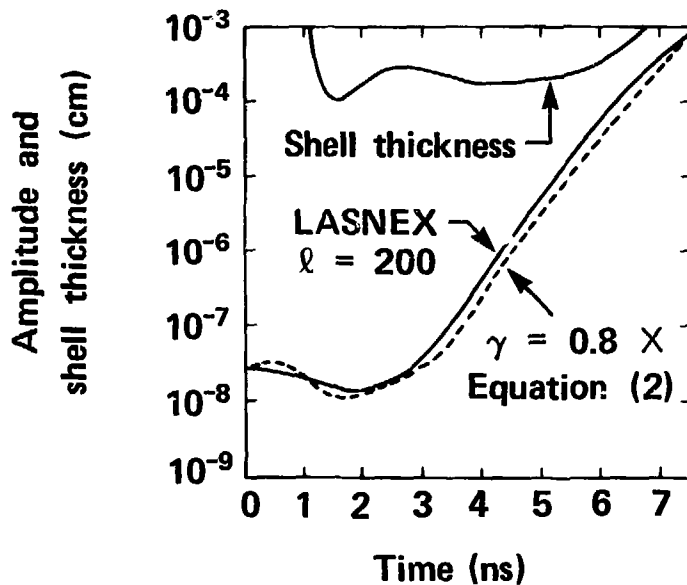
Figure 9

TARGET DESIGN B — TARGET SURVIVES
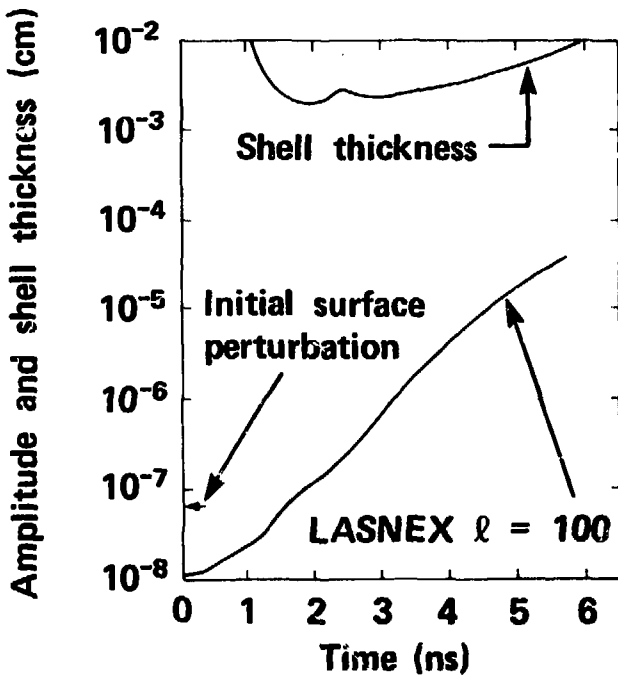
FIGURE 10

TARGET DESIGN C – TARGET SURVIVES
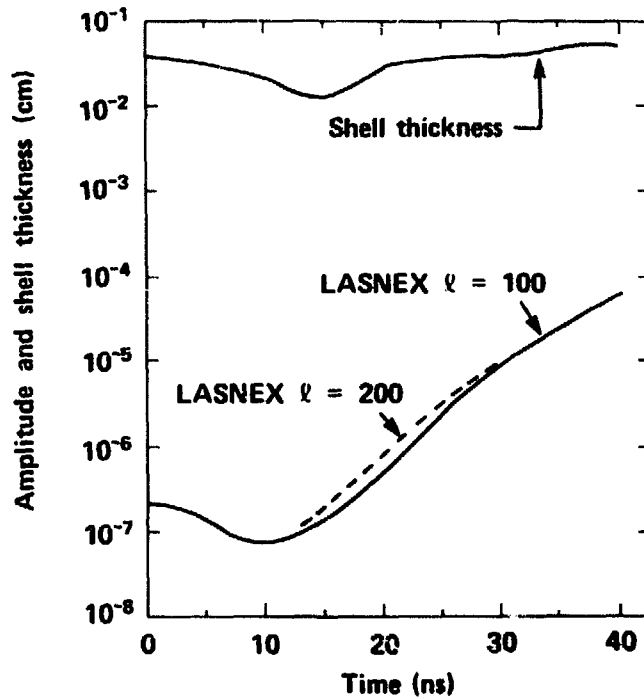
FIGURE 11

TARGET DESIGN D — TARGET SURVIVES
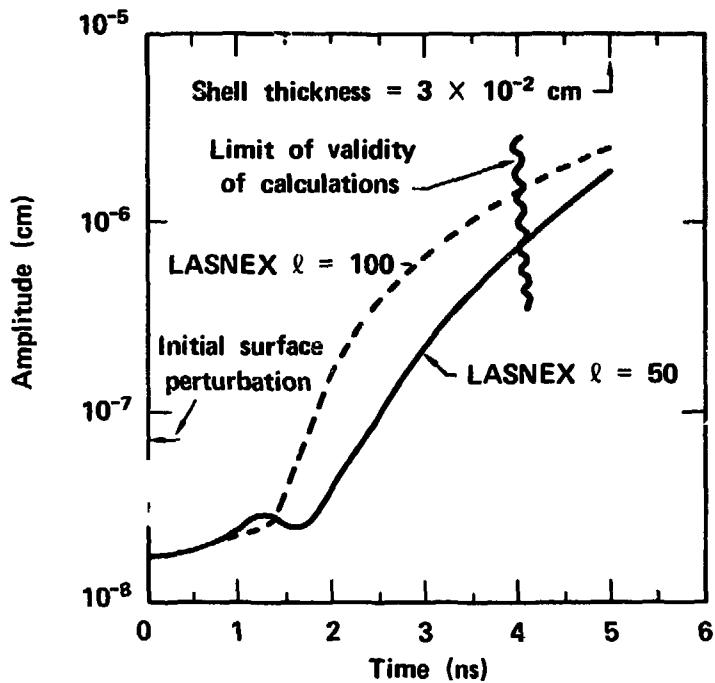
FIGURE 12

COMPARISON OF ELECTRON AND PROTON DEPOSITION PROFILES
Electron Deposition is Strongly Influenced by Multiple Scattering and Bremsstrahlung.
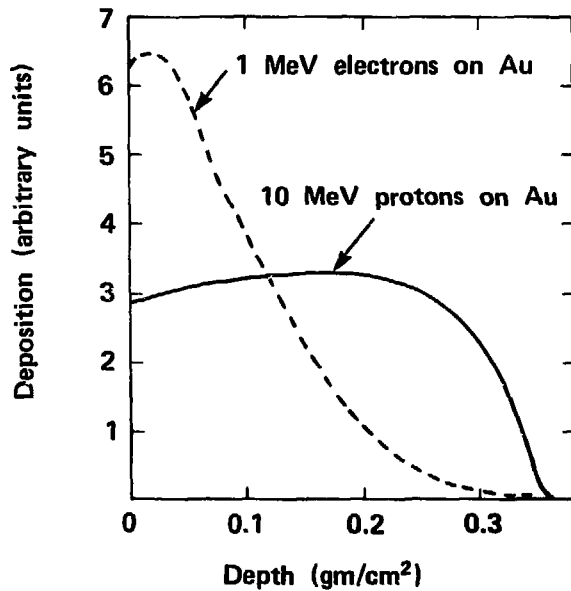
Figure 13

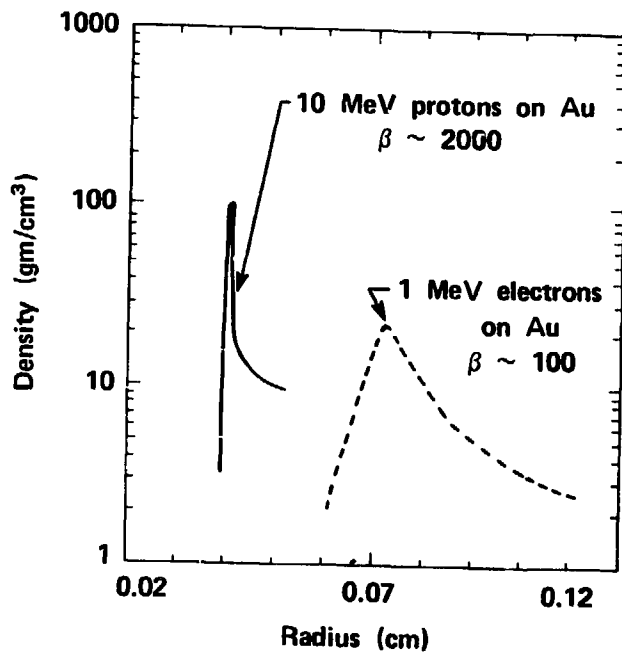## 10 MeV PROTONS PRODUCE A MUCH LARGER DENSITY GRADIENT THAN 1 MeV ELECTRONS.

FIGURE 14

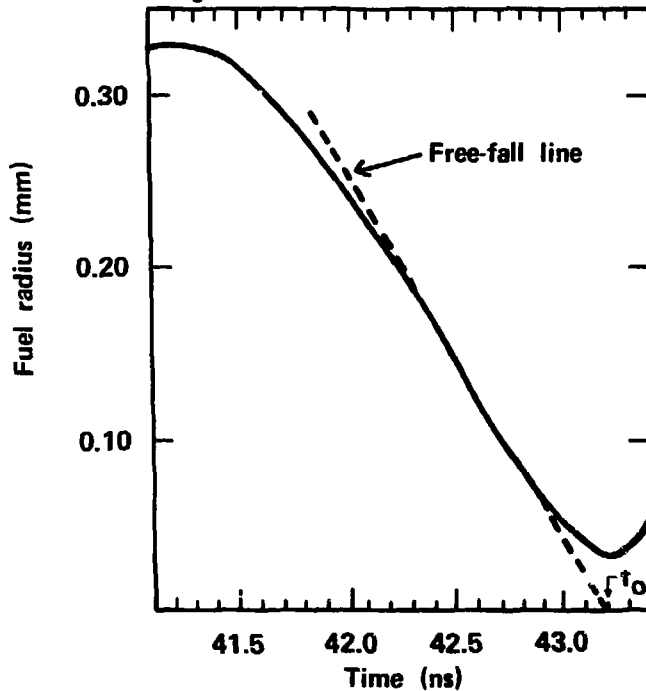PUSHER MATERIAL CAN REACH r = 0 at t = t_0. IGNITION SHOULD OCCUR BEFORE t = t_0.

FIGURE 15

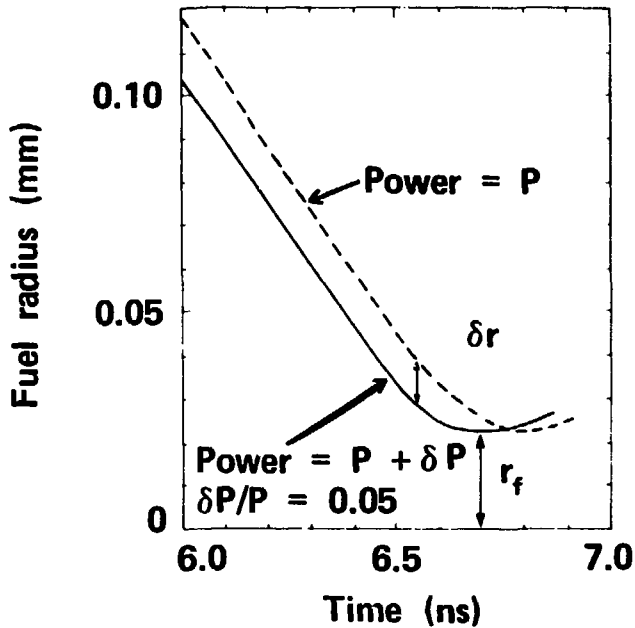# FUEL RADIUS AS A FUNCTION OF TIME FOR TWO DIFFERENT INPUT POWERS

FIGURE 16